Micromechanical characterization of Single-Walled Carbon Nanotube reinforced ethylidene norbornene nanocomposites for self healing applications.

B Aïssa [1,2,*], E Haddad [1], W Jamroz [1], S Hassani [2], R D Farahani [2], P G Merle [3], D Therriault [2,*]

[1] Department of smart material and sensors for space missions. MPB Technologies Inc., 151 Hymus Blvd., Montreal, Canada, H9R 1E9.
[2] Center for Applied Research on Polymers (CREPEC), Mechanical Engineering Department, École Polytechnique de Montréal, P.O. Box 6079, Station 'Centre-Ville', Montreal, Canada. H3C 3A7.
[3] Concordia Center for Composites, Department of Mechanical and Industrial Engineering, Concordia University, Montreal, Quebec, Canada, H3G 2M8.

*Emails addresses: daniel.therriault@polymtl.ca (D. Therriault), brahim.aissa@mpbc.ca (B. Aïssa).

Abstract

We report on the fabrication of self healing nanocomposite materials, consisting of single-walled carbon nanotube (SWCNT) reinforced 5-Ethylidene-2-norbornene (5E2N) healing agent -reacted with Ruthenium Grubbs catalyst- by means of ultrasonication, followed by a three-roll mixing mill process. The kinetics of the 5E2N ring opening metathesis polymerization (ROMP) was studied as a function of the reaction temperature and the SWCNT loads. Our results demonstrated that the ROMP reaction still effective in a large temperature domain (-15 to 45 ºC), occurring at very short time scales (less than one minute at 40 ºC). On the other hand, the micro-indentation analysis performed on the SWCNT/5E2N nanocomposite materials after its ROMP polymerization were shown a clear increase in both the hardness and the Young modulus -up to nine times higher than that of the virgin polymer- when SWCNT loads range only from 0.1 to 2 wt. %. This approach demonstrated here opens new prospects for using carbon nanotube and healing agent nanocomposite materials for self-repair functionality, especially in space environment.

1. Introduction

The presence in space of micrometeoroids and orbital debris, particularly in low earth orbit, presents a continuous hazard to orbiting satellites, spacecrafts and the International Space Station (ISS). Space debris includes all non-functional, man-made objects and fragments, in earth orbit. As the population of debris continues to grow, the probability of collisions that could lead to potential damage will consequently increase. The self healing of impacted composites in space could be the right answer to the mentioned issues.

Indeed, the development of self-healing materials is now being considered for real engineering applications. This new class of material has the ability repair, in which damage triggers an autonomic healing response [1-4]. This new self healing materials-concept offers the designer an ability to incorporate secondary functional materials capable of counteracting service degradation whilst still achieving the primary, usually structural, requirement. In fact, over the past few decades, there has been a growing interest in materials that can self-heal, as this property can increase a materials lifetime, reduce replacement costs, and improve product safety.

The first choice of healing agent, dicyclopentadiene (DCPD) [5-6], was made in the basis of its low cost, long life, low viscosity and volatility, and its polymerization at ambient conditions upon contact with a suitable catalyst [7]. In the event of a crack, the microcapsule shell containing monomer will break, releasing the DCPD into the crack plane which will eventually react with the catalyst to bond the damages. This concept was initially developed for materials in aeronautics [8-11]. The catalyst chosen was first generation Grubbs catalyst: bis (tricyclohexylphosphine) benzylidene ruthenium (IV) dichloride. Grubbs catalyst is well known for promoting olefin metathesis, showing high activity while being tolerant of a wide range of functional groups.

Another similarly reactive diene-containing monomer was investigated as a possible alternative healing agent; for example, ethylidene norbornene (ENB) reacts much faster in ROMP than DCPD [12-15], and also has a much lower freezing point than that of DCPD (which is around 15 $^{\circ}$C), which is more

suitable for space environment. The drawback to using this monomer, however, is that the resulting polymer is linear and thus has inferior mechanical properties as compared to DCPD. Liu et al. [16] tested a system that used a blend of the two monomers as the liquid healing agent to increase the rate of polymerization and range of usable temperatures, while at the same time, maintaining desirable mechanical properties. The polymerization was indeed faster with the addition of ENB, and could be completed at a lower catalyst loading. A sample containing a blend of DCPD/ENB showed the highest rigidity after 120 min of cure time, as compared to studies with the pure monomers and varied ratios of them. DCPD and ENB are presumably responsible for increases in rigidity and reactivity.

Here we report an innovative alternative approach to overcome the lack of the mechanical properties inherent to the ENB based polymers. We have developed a self healing materials consisting of single-walled carbon nanotube (SCWNT) and 5-ethylidene-2-norbornene (5E2N), reacted with ruthenium Grubbs catalyst (RGC). The kinetics of the 5E2N- (ROMP) was shown to still effective in a large temperature domain (-15 to up 45 ºC), with an excellent monomer conversion rate occurring at very short time scale. More importantly, micro indentation analysis have shown an increase in both the hardness and the Young modulus -up to nine times higher than that of the virgin polymer- when SWCNT loads range only from 0.1 to 2 wt. %. This approach demonstrated here opens new prospects for using carbon nanotube and healing agent nanocomposite materials for self-repair functionality, especially in space environment.

2. Experimental details

2.1 Carbon nanotube synthesis process:

Single walled carbon nanotubes (SWCNTs) materials have been synthesized by using the developed plasma torch technology (detailed process can be found in our Refs. [17-18]). In this approach, a carbon containing ethylene (C_2H_4) substance combined with gaseous catalyst based ferrocene ($Fe(C_5H_5)_2$) vapour are injected in an inert gas plasma jet. The inert gas is a mixture of 50 % argon with 50 % helium. The hot temperature of the plasma (~ 5000 K) is capable to dissociate the ethylene and ferrocene

molecules to produce iron and carbon vapour. These atomic and molecular species are the rapidly cooled to a rate of 10^5 K/s in a warmer environment of about 1273 K. The process is exclusively producing SWCNT materials, and the growth takes place in the gas-phase. The as-grown sootlike SWCNTs were purified by an acidic treatment through refluxing in a 3M-HNO_3 (Sigma Aldrich) solution for 5 hours at 130 ^oC, and subsequently filtered (Filter type-GV, Millipore Corp.).

The plasma-grown carbon nanotubes were characterized by scanning electron microscopy (SEM) using a Jeol JSM-6300 F microscope. Bright field transmission electron microscopy (TEM) images were obtained using a Jeol JEM-2100 F FEG- TEM (200 kV) microscope. The Raman measurements were performed with the 514.5 nm (2.41 eV) laser radiation of an Ar^+ laser focused onto the sample with a spot of 1 µm (microRaman spectroscopy, Renishaw Imaging Microscope Wire ^{TM}). The Raman spectra were taken with a backscattering geometry at room temperature in the 100–2000 cm^{-1} spectral region.

2.2 Nanocomposite fabrication and tests:

All the chemicals (Ruthenium Grubbs catalyst (RGC) first generation, 5E2N monomer, Epon 828 resin epoxy, etc.), were purchased from Sigma-Aldrich and used as received. The weighed amount of purified SWCNT was first dispersed in a solution of 5E2N. The resulting nanocomposites containing different mass fraction of SWCNT were passed several times in a three-roll mixing mill (Exakt 80E, Exakt Technologies Inc.) where the gap between the rolls and the speed of the apron roll has adjusted according to the method described by Thostenson and Chou [19]. The total procedure consisted of five passes at a gap of 25 µm and with a speed of 200 RPM, five passes at a gap of 15 µm with a speed 200 RPM and finally nine passes at a gap of 5 µm with a speed 250 RPM. The nanocomposite solution was finally subjected to an ultrasonication step (ultrasonic cleaner 8891, Cole-Parmer) for 30 minutes. In parallel, a ruthenium Grubbs catalyst powder (sigma Aldrich) was mixed with an organic solution of dichloromethane DCM (sigma Aldrich) and subjected to the same mechanical blending process as for the SWCNT. After solvent evaporation, the fine RGC powder was slowly added in the nanocomposite solution containing SWCNT over a gentle stirring (model SP131825, Barnstead international), and the obtained nanocomposites samples were immediately placed in a Tenney Junior Environment Chamber ^{TM}

under air, where the time of polymerization was evaluated starting from this final step. Doing so, the ROMP reactions were then performed at different temperatures ranging from -15 to 45° C.

The microscopic scale dispersion was characterized by observing a 1 mm thick film under a transmission light optical microscope using the 40× objective (BX-61, Olympus) and image analysis software (Image-Pro Plus, Media Cybernetics Inc.). The elemental chemical bonding of the samples were investigated by X-ray photo- electron spectroscopy (XPS), performed at room temperature and at a base pressure of 10^{-9} mbar, with the ESCALAB 220i-XL system, using monochromatic Al Ka radiation as the excitation source (1486.6 eV, full width at half-maximum of the Ag 3d 5/2 line=1eV at 20 eV pass energy). The reported binding energies were calibrated with respect to the C 1s line at 284.5 eV.

After their full polymerization, the mechanical properties of the obtained 5E2N/CNT nanocomposites were characterized by depth sensing indentation using a commercially available CSM Micro Indentation Tester, equipped with a Vickers diamond tip. The applied loads were 3 N. Hardness, H and Young's modulus, E, for each sample, were obtained from a minimum of 10 indentations tests.

3. Results and discussion

3.1 Single walled carbon nanotubes characterization:

Fig. 1 (a) shows a representative TEM micrographs of the as-grown SWCNT deposit, where bundles of a few single-walled nanotubes (the diameter of the individual tubes is about 1.2 nm) are clearly seen. In conjunction with the SWCNTs, other carbon nanostructures (e.g., nanocages, nanonions, and nanohorns) can be also produced by the plasma torch process. Metal catalyst nanoparticles (NPs) are also expected to be present in the as-grown deposits. The darker spots of Fig. 1 (a) represent Fe metal catalyst particles and/or Fe NPs wrapped within carbon nanostructures (shown by black arrows). The nanotubes purification permits indeed to eliminate a large part of the catalyst residues and other carbon nanostructures having a high density of structural defects, as illustrated in Fig. 1(b). The purified (PF)-SWCNTs consist of bundles having diameters in the 2–10 nm range and lengths in the order of few µm

leading thereby to aspect ratios of at least three orders of magnitudes. A typical Raman spectrum (figure 1 (c)) of the purified nanotubes materials shows clear scattering peaks appearing in the low (100–300 cm^{-1}) and high (~1600 cm^{-1}) frequency regions, corresponding to the radial breathing mode (RBM) and the tangential vibrating mode (G), respectively, which are the fingerprints of the presence of SWCNTs. The RBM peak centered at 185 cm^{-1} is attributed to the strong presence of single walled carbon nanotubes having a mean diameter of 1.2 nm according to the formula of Bandow *et al.* [20]. The D-peak centered around 1350 cm^{-1} is due to the presence of amorphous and/or disordered carbon structures. Nevertheless, the rather very low D-to-G peak intensity ratio (~0.05) is worth noting, which indicates the overall high quality of the SWCNTs mats. The TEM observations are well consistent with the Raman results, pointing out the single walled structure of the grown CNT as well as their narrow diameter.

3.2 Ring opening metathesis polymerization of the nanocomposite:

Figures 2 (a-b) show the typical optical and SEM micrographs of the as-received Grubbs catalyst, respectively, showing rods up to ~120 µm in length and ~ 30 µm in width. Fig. 2 (d) shows the typical XPS survey spectrum of the Grubbs catalyst dispersed into the CNT/5E2N monomer solution -by using a three-roll mixing mill (see Fig. 2 (c))- after its ROMP polymerization process. One can note that the main components of the Grubbs molecules, namely, ruthenium (Ru $3p_{3/2}$ and Ru $3p_{1/2}$ at 463 and 485 eV, respectively), phosphor (P_{2p} and P_{2s} located at 132 and 190 eV, respectively), and chlorine (Cl 2p and Cl 2s, located at 200 and 276.5 eV, respectively) are well identified in the nanocomposite, which suggests strongly that the catalyst still keep its original stoichiometry after its mixture. On the other hand, the SEM data show that the catalyst sizes decrease down to 200-500 nm, and it shapes seem more spherical in appearance (Fig. 2(c)).

To point out the kinetics of the polymerization reaction as a function of the temperature and the SWCNT concentrations, we have performed ROMP reactions tests at temperatures ranging from -15 to 45 ^{o}C, and CNT loads ranging from 0 to 5 wt. %. Figure 3 illustrates the time needed to the 5E2N polymerization (ROMP) as a function of the reaction temperature. This time is found to be 146 minutes at -15° C, while it decreases to 4 min only when the reaction temperature increases to 20° C. The

polymerization occurs then at very short time (as low as 0.2 min) when the temperature is increased to 45° C. It is worth noted here that no significant change in the kinetics of the ROMP reaction was observed with respect to the CNT loads (times values are within the experience uncertainties error bar). In sum, at room temperature, the ROMP reaction of the 5E2N monomer triggered by the Grubbs catalyst is found to happen at a very short time scales (less than 5 minutes). The 5E2N monomer provided definitely the best polymerization time over the alternative monomers [21].

3.3 Micromechanical nanocomposite testing:

Micro/nanoindentation is now commonly used to investigate mechanical properties of materials at the micro/nanoscale. This is a straightforward technique which can be used to measure mechanical properties of polymer bulks and thin films. The micro hardness test is based on the standards for instrumented indentation, ASTM E2546 and ISO 14577. It uses an established method where an indenter tip with a known geometry is driven into a specific site of the material to be tested, by applying an increasing normal load. When reaching a pre-set maximum value, the normal load is reduced until partial or complete relaxation occurs. This procedure is performed repetitively; at each stage of the experiment the position of the indenter relative to the sample surface is precisely monitored with an optical non-contact depth sensor.

For each indentation, the applied load value is plotted with respect to the corresponding position of the indenter. The resulting load/displacement curves provide data specific to the mechanical nature of the material under examination, and from these obtained load-displacement data, many mechanical properties such as hardness, and elastic properties (E) can be determined [22]. In sum, the mechanical properties are determined based on the mechanical response of the specimen to the applied load as well as the indenter geometry [22-24].

We have used in the present work an indenter type of Vickers Diamond shape. Established models are used to calculate quantitative hardness and modulus values for such data. In fact, the system was equipped with an automatic computation method of Oliver & Pharr with its specific software giving directly the mechanical properties.

The Hardness and the Young modulus are the two main mechanical properties frequently determined using indentation techniques. As the indenter is pressed into the sample, both elastic and plastic deformation occurs and a hardness (H) impression conforming to the indenter geometry is formed. Only the elastic portion of the displacement is recovered during indenter withdrawal which enables the calculation of elastic modulus. Micro/nanohardness is defined as the indentation load divided by the estimated contact area of the indentation. The static mechanical characterization of CNT/5E2N nanocomposites was performed with this technique [24]. Indeed, the mechanical properties of CNT/5E2N nanocomposite having a CNT loads ranging from 0 to 5 wt. % were characterized. Typical example of the load-displacement curves obtained for 3N load is shown in Fig. 4 (a) while the post-indentation residual impressions optical images of pure 5E2N (i.e., 5E2N monomer reacted with RGC and 0 wt. % of CNT) and 5E2N loaded with 2 wt. % of CNT are shown in Figs. 4 (b) and (c), respectively.

All the deduced mechanical properties are summarized in the table of Fig. 5 (a). When higher loads were applied, both H and E increased with CNT loads. Compared to pure 5E2N polymer (i.e., for 0 wt. % CNT), analysis of micro-indentation results show that CNT/5E2N exhibits a higher elastic strain to failure and resistance to plastic deformation, expressed by the H/E and the H^3/E^2 ratios, respectively.

Table of Fig. 5(a) summarizes the Hardness (H), Young modulus (E), elastic strain (H/E) and the resistance to plastic deformation (H^2/E^2) of the neat 5E2N polymer and its nanocomposite samples as a function of the nanotube contents. A clear improvement in all mechanical properties, comparatively to that of neat 5E2N samples, is obtained for CNT load as low as 0.1 wt. %, and continues to increase with increasing the nanotube content (for example, an enhancement as high as 900 % is obtained in case of hardness for a CNT load of 2 wt. % only), indicating unique reinforcing effects of nanotubes [24].

Indeed, the incorporation of CNT fillers may act as a cross-linking network inside the 5E2N polymer and consequently leads to an increase of its overall mechanical properties. However, it is noteworthy to mention that at 5 wt. % of CNT load, samples do not show any further improvement as compared to these observed for the 0.1-2 wt. % interval, as shown by the plots of Figs. 5 (b) and (c).

These results can be explained by the fact that, the high surface area of carbon nanotubes

increases with respect to their concentration in the nanocomposite. At 5 wt. %, there is highly likely less available polymer to be well intercalated into the CNT bundles. Consequently, the interactions between the nanotubes are much higher at this load, giving rise to the formation of aggregates. The aggregation of nanotube bundles decreases the effective content of SWCNTs in the polymer matrix. At this load, these aggregates may cause SCWNT pull-out, break-off, break-out or snagging in the samples, that are directly responsible for the obtained mechanical properties -which still below their theoretically predicted potential- [25]. Moreover, the quantity of aggregates increases with respect to the nanotube concentration, preventing further interaction of the polymer with SWCNTs [23], and probably, the only outside nanotubes of a bundle can be bonded to the polymer matrix. The inside nanotubes are weakly interacting by van der Waals attraction. The nanotubes within a bundle can easily slide past each other and the shear modulus of the carbon nanotube bundles is relatively low [27]. This is one of the reasons why the mechanical properties of the higher SWCNT concentrations are significantly decreased [25]. For low nanotube concentrations (i.e., less than 2 wt. %), an intercalation of the polymer inside SWCNT bundles could be enabled, helping thereby the nanotube dispersion. Thus, interactions between nanotubes are low and the bundles can be desegregated. In sum, the existence of CNT aggregates at higher concentrations is believed to be responsible for the relatively low hardness and Young modulus, as compared to that expected with theoretically predicted values [25]. It's worth noting here that the theoretical predictions of strength and elastic modulus are almost all for single nanotubes that are well dispersed in a matrix, whilst calculations based on experiments have not yet well addressed the possibility of relative slippage of the individual tubes within a bundle as well as the aggregation of carbon nanotube bundles. For that, these hypotheses have to be taken with high care, and more quantitative characterizations (such a cryo-microtome with respect to the CNT loads) are needed to support our claims. Intercalation of polymer into the bundles is one of the key reinforcing mechanisms atwork in the SWCNT polymer nanocomposites, and better dispersion techniques are inevitably needed to overcome such mentioned limitations. Finally, the fact that the mechanical properties start to change for a CNT load as low as 0.1 wt. % highly likely

suggest that both mechanical and/or the electrical percolation thresholds could be –at least- around this value.

3.4 Elaboration of the 3D microvascular network and self healing testing:

Three-dimensional micro-scaffolds were fabricated using a computer-controlled robot (I & J2200-4, I & J Fisnar) that moves a dispensing apparatus (HP-7X, EFD) along the *x*, *y* and *z* axes [28]. The fabrication of the microscaffold began with the deposition of the ink-based filaments on an epoxy substrate, leading to a two-dimensional pattern. The following layers were deposited by successively incrementing the *z*-position of the dispensing nozzle by the diameter of the filaments. The 3D microscaffold consisted of eleven layers of fugitive ink filaments, deposited alternatively along and perpendicular to the scaffold longitudinal, *x*, axis. The filament diameter was 150 μm for a deposition speed of 4.7 mm/s at an extrusion pressure of 1.9 MPa. The overall dimensions of the 3D ink structure were 62 mm in length, 8 mm in width and 1.7 mm in thickness with 0.25 mm spacing between filaments. The empty space between the scaffold filaments was filled with the same epoxy resin used for the substrate fabrication (i.e., Epon 828/Epikure 3274, Miller-Stephenson Chemical Co.), mixed with the fine powder of the Grubb's catalyst particle. Upon the curing of the epoxy, the fugitive ink was removed from the structure by the liquefaction at 100 °C and applying vacuum, yielding an interconnected 3D microfluidic network. Figures 6 (a)-(d) schematically illustrate the fabrication process.

The 3D-reinforced beams were produced by micro-injecting the empty microfluidic networks with the liquid nanocomposites (5E2N/CNT) having a CNT load of 0.5 wt. %. The materials injected behave like micro-scale fibers inside a matrix of epoxy/RGC Grubb's nanoparticles. Fig. 6 (e) schematically illustrates the micro-injection step for a nanocomposite-injected beam. The nanocomposites were injected into the empty channels using a fluid dispenser (EFD800, EFD) via a plastic tube connected to the end of the beams and the fluid dispenser at both ends. The injection pressure was adjusted at 400 kPa, which led to an injection speed of ~1 mm/s. The final specimen was then sealed to protect the liquid nanocomposite inside the sample.

Figure 7 (a) shows an optical top-view image of a micro-vascular nanocomposite infiltrated network just after the impact damage (hole), caused by low velocity dropping mass (Impact Energy ~ 23 J). In Fig. 7 (b) we can see the microvascular sample heated at 60 ^{o}C for 15 minutes, where the impact damage seems to be totally filled by the liquid 5E2N/SWCNT nanocomposite healing-agent, and is completely solidified after 30 minutes (Fig. 7 (c)). In fact, the liquid 5E2N/SWCNT nanocomposite was released after the impact event and met the RGC nanoparticles already embedded into the epoxy scaffold where the ROMP reaction has taken place. We can clearly see in the cross sectional view (Fig. 7 (d)) the polymerisation of the 5E2N/SWCNT nanocomposite inside the damage-zone. On the other hand, the Raman spectrum performed directly on the damage-zone, before the impact event (i.e., on the undamaged epoxy scaffold) and after the complete healing process (where the damage hole was completely filled and completely solidified) is shown in Fig. 7 (e). The presence of the SWCNT materials in the repaired damage is clearly confirmed by the RBM, D and G Raman peaks.

After this proof of concept step, it can be seen that the self-healing system in the study has a potential to be used in practical application. Self-healing has most benefit for structures where good durability and long service life are important, or for structures that are difficult to reach for inspection and maintenance. More efforts will be done to characterize mechanically the healing efficiency of our microvascular devices as a function of the nanotubes loads, the damage morphology (i.e, the geometry and the shape of the impact zone), together with the dynamic of the healing reaction itself.

4. Summary

A self healing nanocomposite materials consisting of single-walled carbon nanotube (SCWNT) and 5-Ethylidene-2-norbornene (5E2N), reacted with ruthenium Grubbs catalyst, were successfully prepared using ultrasonication, followed by a three-roll mixing mill process. The kinetics of the 5E2N was found to still effective in a large temperature domain (-15 to up 45 ºC), where the ROMP reaction was shown to occur at a very short time scale (less than one minute at 45 ºC). Moreover, the micromechanical characterization performed on the SWCNT/5E2N nanocomposite materials after its

ROMP polymerization have shown a clear improvement in the entire mechanical properties of the polymer, where an increase in both the hardness and the Young modulus -up to 9 times higher than that of the virgin polymer- was systematically observed for CNT loads ranging only from 0.1 to 2 wt. %. Intercalation of polymer into the bundles is one of the key reinforcing mechanisms atwork in the SWCNT polymer nanocomposites. Our obtained results open definitely new prospects for using carbon nanotube and healing agent nanocomposite materials with higher mechanical characteristics for self-repair functionality, especially in space environment.

Acknowledgment

The authors would like to gratefully acknowledge the assistance of the Canadian Space Agency for this work, and the financial contribution of the Natural Science and Engineering Research Council (NSERC) of Canada, and the Fonds Québécois de la Recherche sur la Nature et les Technologies (FQRNT).

References

[1] Dry C 1996 *Compos. Struct.* **35** 263

[2] Li V C, Lim Y M and Chan Y W 1998 *Compos. Part B* **29** 819

[3] Pang J W C and Bond I P 2005 *Compos Part A* **36** 183

[4] Rule J D, Sottos N R and White S R 2007 *Polymer* **48** 3520

[5] White S R, Sottos N R, Geubelle P H, Moore J S, Kessler M R, Sriram S R, Brown E N and Viswanathan S 2001 *Nature (london)* **409** 794

[6] Brown E N, Kessler M R, Sottos N R and White S R 2003 *J. Microencapsul* **20** 719

[7] Jones A S, Rule J D, Moore J S, Sottos N R and White S R 2007 *J. R. Soc. Interface* **4** 395

[8] Sliwka W 1975 *Angew Chem.* **87** 556

[9] Gouin S 2004 *Trends in Food Sci. & Tech.* **15** 7

[10] Lin Y H E and Vasavada R C 2000 *J. microencaps.* **17** 1

[11] Wan L S C, Heng P W S and Chia C G H 1992 *Drug Develop. & Indust. Pharm.* **18** 997

[12] Lee J K, Hong S J, Liu X and Yoon S H 2004 *Macromol. Res.* **12** 478

[13] Liu X, Lee J K, Yoon S H and Kessler M R 2006 *J. Appl.Polym. Sci.* **101** 1266

[14] Sheng X, Kessler M R and Lee J K 2007, *J. Therm. Anal. Calorim.* **89** 459

[15] Liu X, Sheng X, Lee J K and Kessler M R 2007 *J. Therm Anal. Calorim.* **89** 453

[16] Liu X, Lee J K, Yoon S H and Kessler M R 2006 *J. Appl. Polym. Sci.* **101** 1266

[17] Smiljanic O, Stansfield B L, Dodelet J P, Serventi A and Désilets S 2002 *Chem. Phys. Lett.* **356** 189

[18] Smiljanic O, Larouche F, Sun X L, Dodelet J P and Stansfield B L 2004 *J. Nanosci. & Nanotech.* **4** 1005

[19] Thostenson E T and Chou T W 2006 *Carbon* **44** 3022

[20] Bandow S, Asaka S, Saito S, Rao A M, Grigorian L, Richter E and Eklund P C 1998 *Phys. Rev. Lett.* **80** 3779

[21] Wool R P 2008 *Soft Matter* **4** 400

[22] Li X D and Bhushan B 2002 *Mater. Charac.* **48** 11

[23] Valentini L, Biagiotti J, Kenny J M and Manchado M A L 2003 *J. Appl. Polym. Sci.* **89** 2657

[24] Li X, Gao H, Scrivens W A, Fei D, Xu X, Sutton M A, Reynolds A P and Myrick M L 2004 *Nanotechnology* **15** 1416

[25] Mamedov A A, Kotov N A, Prato M, Guldi D M, Wicksted J P and Hirsch A 2002 *Nat. Mater.* **1** 190

[27] Watts P C P, Hsu W K, Chen G Z, Fray D J, Kroto H Wand Walton D R M 2001 *J. Mater. Chem.* **11** 2482

[28] Therriault D, White S R and Lewis J A 2003 *Nature Materials* **2** 265

Figures captions:

Figure 1: Morphology of the grown SWCNTs: (a) Typical Raman spectrum of the as-grown SWCNT materials, where the various RBM, *D* and G bands are clearly identified. The inset shows a close-up of the RBM band located at 185 cm^{-1}, corresponding to an individual SWCNT having a mean diameter of 1.2 nn. The corresponding representative TEM images of (b) the as-grown and (c) purified SWCNT materials. Black arrows in (b) indicate the residual Fe catalyst, and inset in (c) is a HRTEM close-up showing nanotubes of 1.2 nm-diam. in total agreement with the Raman analysis in (a).

Figure 2: Representative (a) optical and (b) SEM micrographs of the as-received Grubbs catalyst showing rods up to ~120 µm in length and ~ 30 µm in width. (c) SEM images of the Catalyst after its 3 roll mixing, showing reducing in catalyst-size together with more spherical particles in appearance, with diameter of about 0.2-0.5 µm. (d) Typical XPS survey spectrum of the Grubbs catalyst dispersed into the 5E2N matrix after its polymerization, where all the Ru, P, and Cl components of the Grubbs molecules are clearly identified.

Figure 3: Time of the 5E2N polymerization (ROMP) as a function of reaction temperature and CNT loads (First generation Grubbs Catalyst, 1 wt. %, in air).

Figure 4: (a) Representative load–displacement curves of indentations made at a peak indentation load of 3 N on the 5E2N and its SWCNT reinforced samples. Post-indentation residual impressions: (b) pure 5E2N reacted with RGC (i.e., 0 wt. % CNT) and (b) 5E2N/CNT (CNT load of 2 wt. %) taken at 3 N.

Figure 5: (a) Table summarizing the whole mechanical properties obtained from Vickers micro indentation at a fixed applied load of 3 N. (b) Plots of the Hardness, and the Young modulus as a function of the CNT loads in the nanocomposites. (c) Plots of the Hardness (*H*), and the Young modulus (*E*) as a function of the CNT loads in the nanocomposites.

Figure 6: Schematic representation of the manufacturing process of a 3D-reinforced nanocomposite beam through micro-injection of 3D microfluidic network: (a) and (b) deposition of fugitive ink scaffold on an epoxy substrate, (c) encapsulation of the 3D ink-based scaffold using epoxy resin containing Grubb's catalyst followed by resin solidification, (d) ink removal at 100° C under vacuum, (e) micro-injection of the empty network by the prepared liquid 5E2N/SWCNT nanocomposite. (*f*) Cut beam to final dimensions.

Figure 7: (a) Optical top-view image of a micro-vascular nanocomposite infiltrated network just after the impact event. (b) Sample heated at 60 ^{o}C for 15 minutes. (c) Sample after 30 minutes at 60 ^{o}C where the liquid healing-agent was completely solidified. (d) Cross sectional view of the healed damage in (c) showing the clear polymerisation inside the hole. (e) Raman spectrum performed directly on the damage zone before impact event and after hole repairing, showing clear presence of the SWCNT materials (see RBM, G and D bands) in the self healed damage.

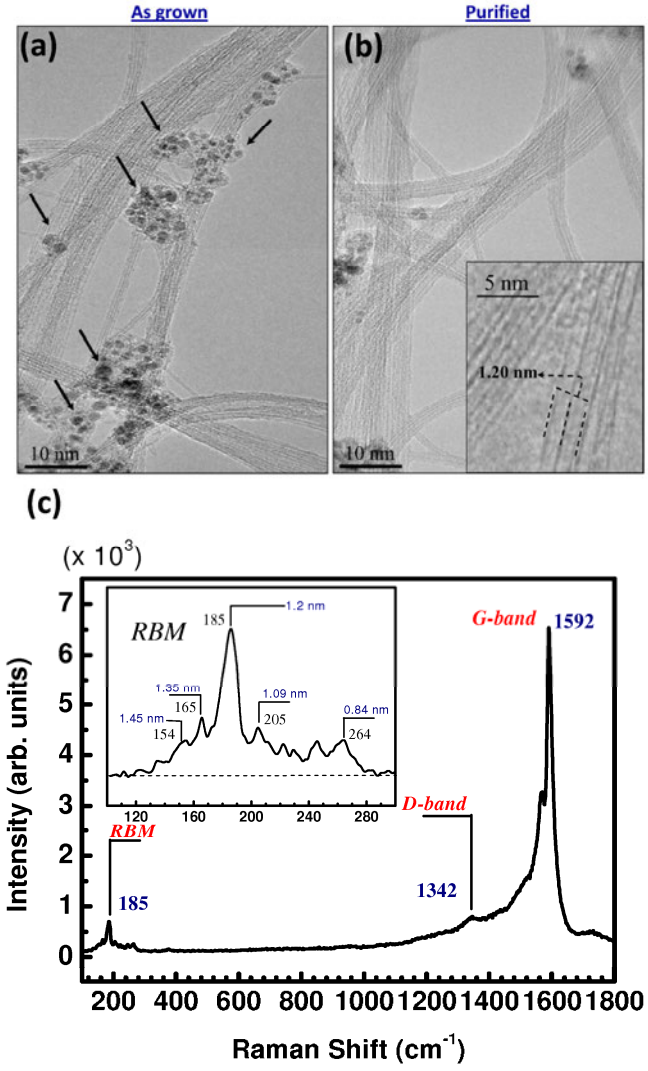
As grown
Purified
(a)
(b)
10 nm
10 nm
5 nm
1.20 nm
(c)
(x 10^3)
Intensity (arb. units)
Raman Shift (cm^-1)
RBM
185
1.2 nm
1.35 nm
165
1.45 nm
154
1.09 nm
205
0.84 nm
264
G-band
1592
D-band
1342
RBM
185

Figure 1.

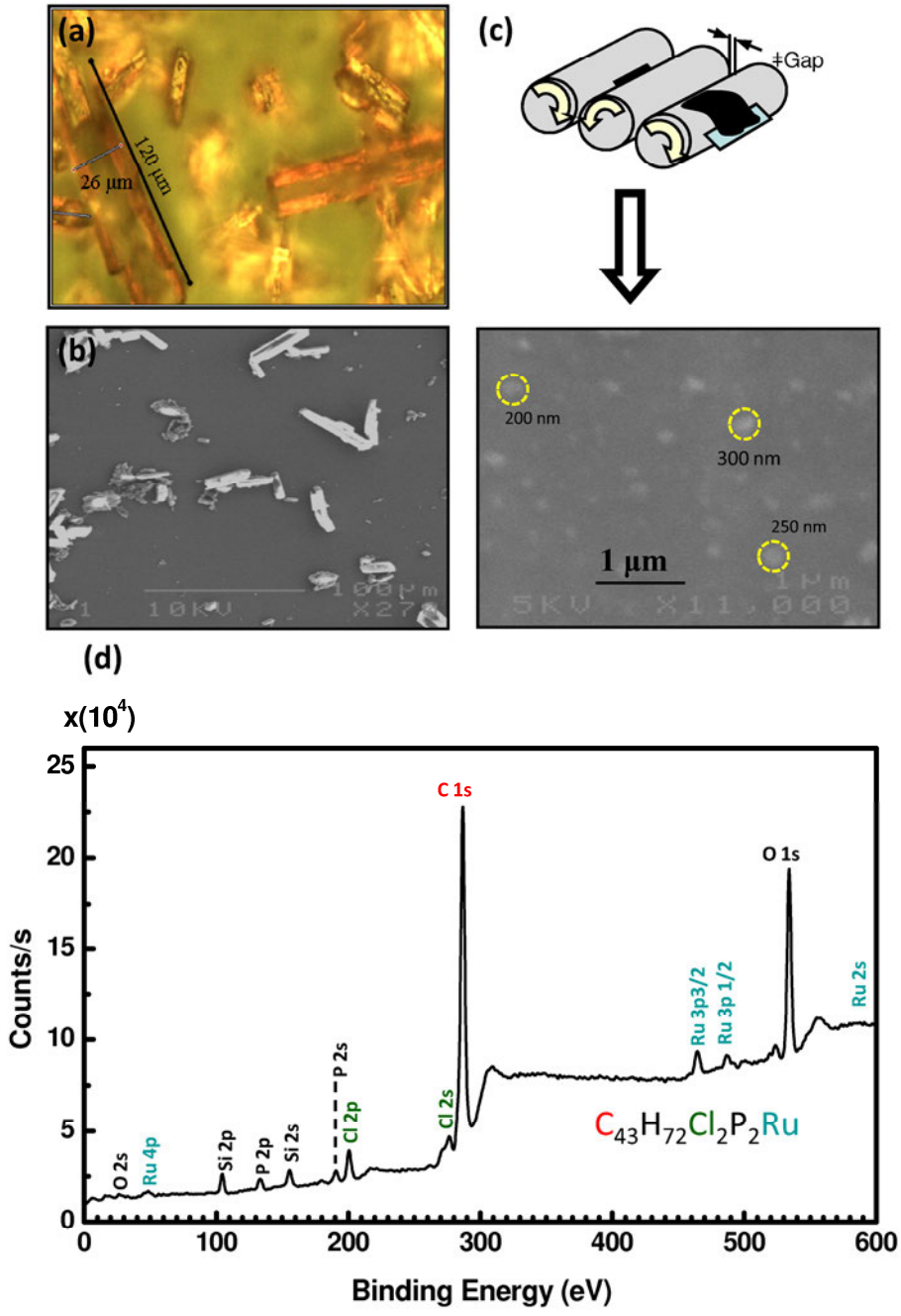
(a)
120 µm
26 µm
(c)
±Gap
(b)
200 nm
300 nm
250 nm
1 µm
(d)
x(10^4)
Counts/s
Binding Energy (eV)
C 1s
O 1s
Ru 2s
Ru 3p3/2
Ru 3p 1/2
Cl 2s
Cl 2p
P 2s
Si 2p
P 2p
Si 2s
O 2s
Ru 4p
C43H72Cl2P2Ru

Figure 2.

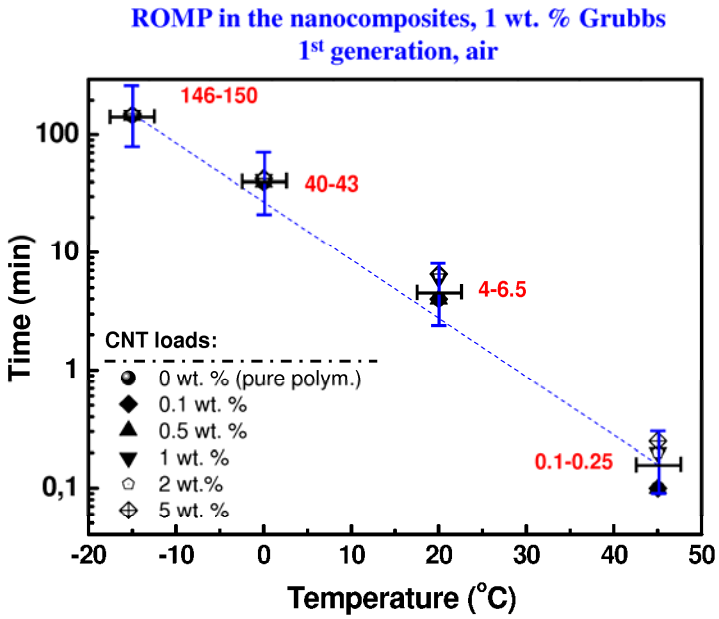
ROMP in the nanocomposites, 1 wt. % Grubbs
1st generation, air
146-150
40-43
4-6.5
0.1-0.25
CNT loads:
0 wt. % (pure polym.)
0.1 wt. %
0.5 wt. %
1 wt. %
2 wt.%
5 wt. %
Time (min)
100
10
1
0,1
-20
-10
0
10
20
30
40
50
Temperature (°C)

Figure 3.

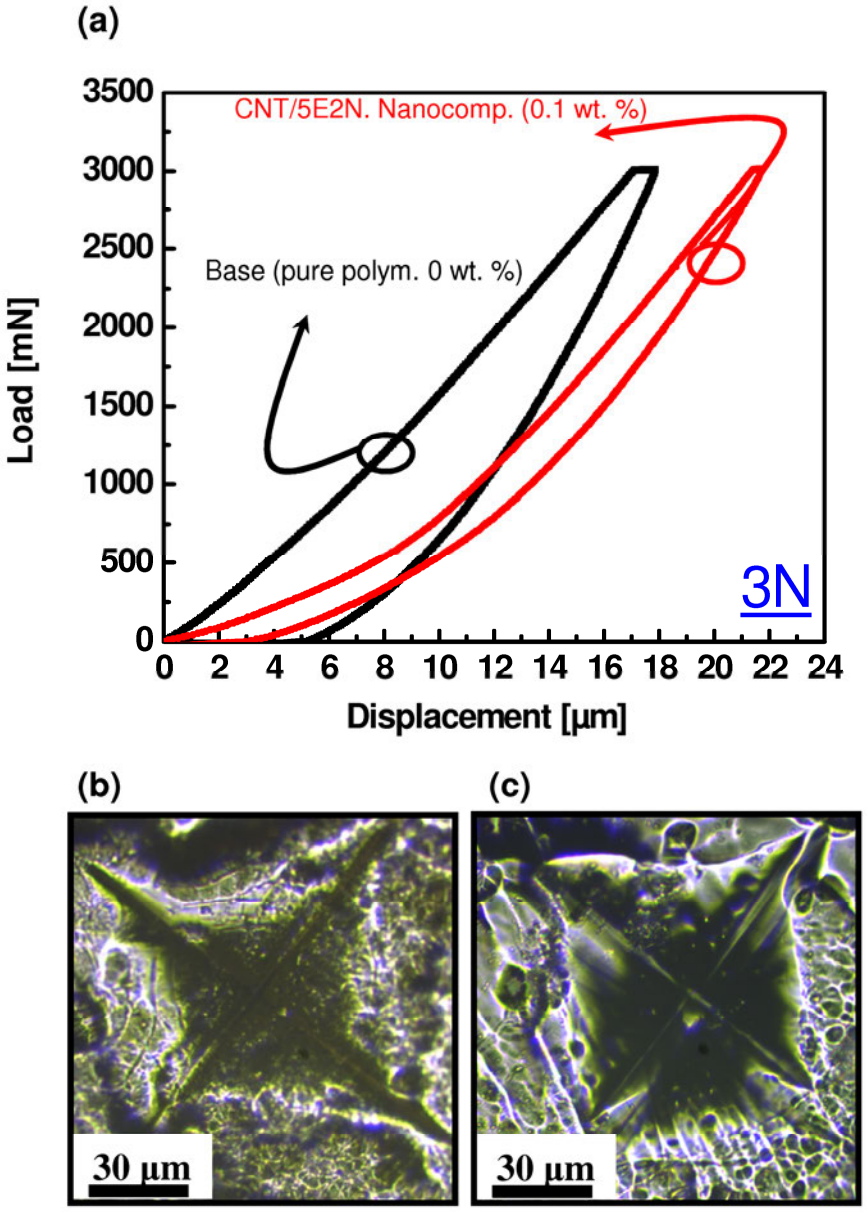
(a)
CNT/5E2N. Nanocomp. (0.1 wt. %)
Base (pure polym. 0 wt. %)
3N
Load [mN]
Displacement [µm]
(b)
(c)
30 µm
30 µm

Figure 4.

(a)

CNT Loads	Hardness, H [GPa]	Young's modulus, E [GPa]	Elastic strain to failure, H/E	Resistance to plastic deformation, H^2/E^2[GPa]
Virgin sample (0 wt. %)	0.4	3.6	0.11	0.0123
Load 1: 0.1 wt. %	1.3	5.9	0.22	0.0485
Load 2: 0.5 wt. %	1.9	8	0.23	0.0564
Load 3: 1 wt. %	2.7	11	0.24	0.0602
Load 4: 2 wt. %	3.6	14	0.25	0.0661
Load 5: 5 wt. %	0.8	4.6	0.17	0.0302

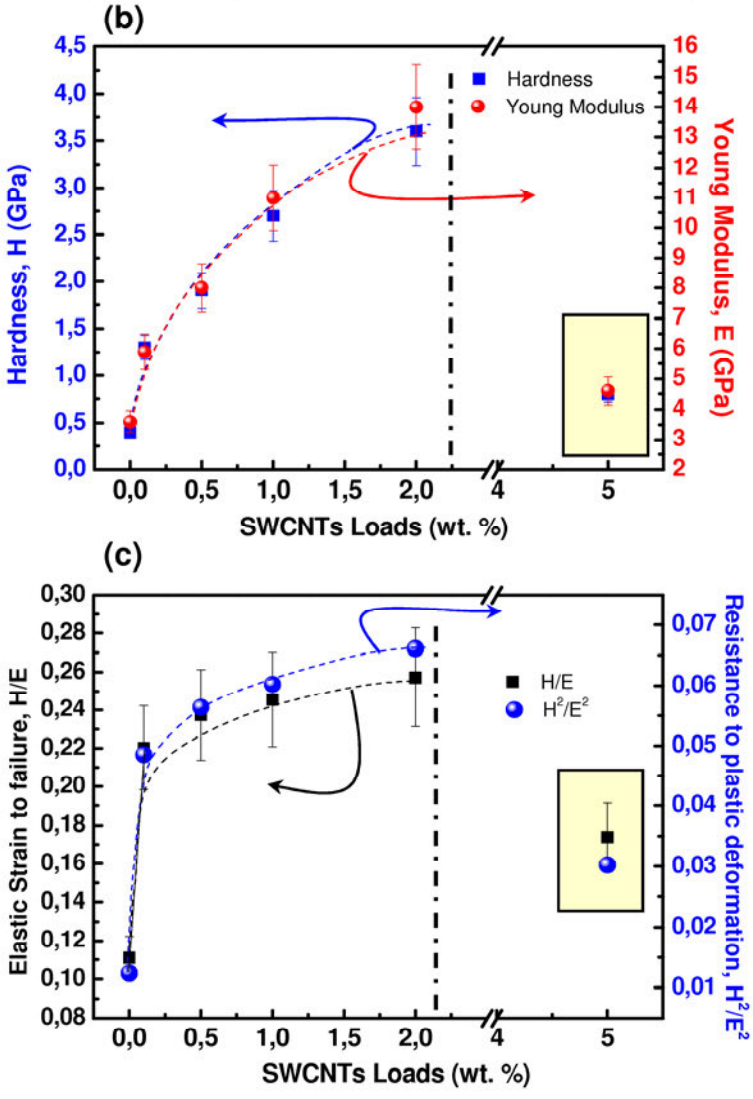

Figure 5.

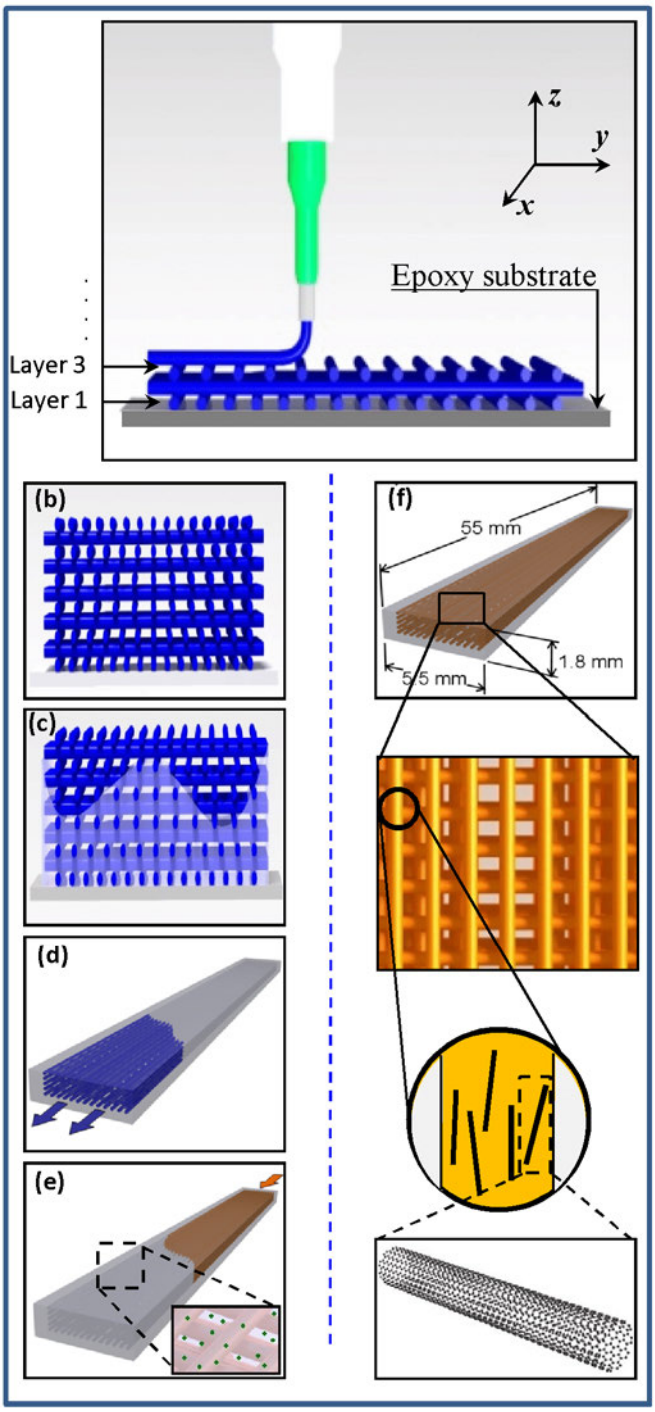

Figure 6.

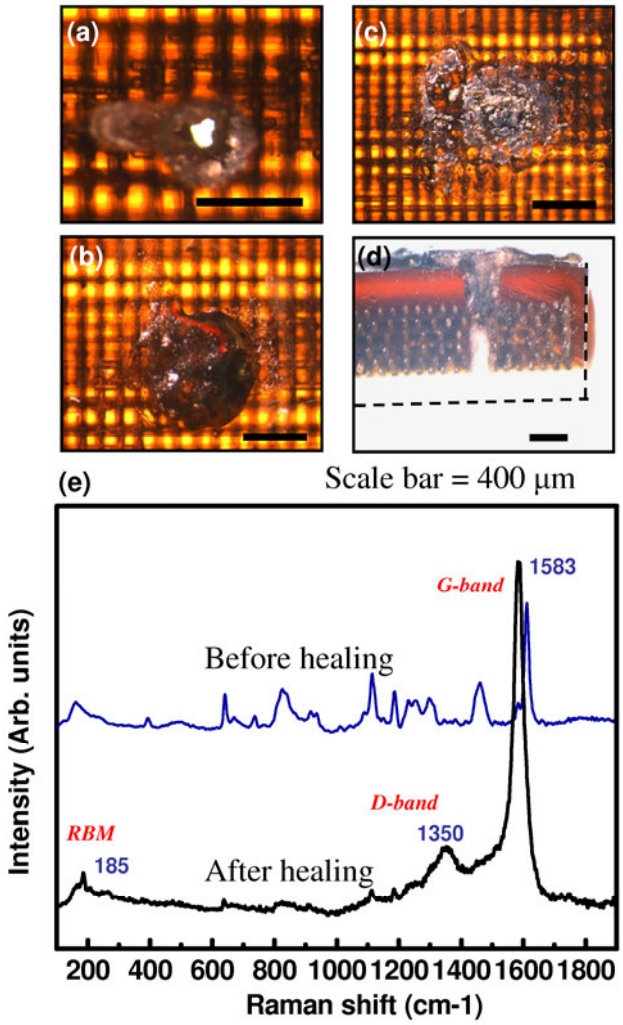
(a)
(c)
(b)
(d)
Scale bar = 400 μm
(e)
G-band
1583
Before healing
D-band
1350
RBM
185
After healing
Intensity (Arb. units)
200 400 600 800 1000 1200 1400 1600 1800
Raman shift (cm-1)

Figure 7.